Metallogels from Glycolipid Biosurfactant

Alexandre Poirier, Patrick Le Griel, Javier Perez, Daniel Hermida-Merino, Petra Pernot, Niki Baccile

Metallogels from Glycolipid Biosurfactant

Alexandre Poirier,[a] Patrick Le Griel,[a] Javier Perez,[b] Daniel Hermida-Merino,[c] Petra Pernot,[d] Niki Baccile,[a,*]

[a] Sorbonne Université, Laboratoire de Chimie de la Matière Condensée de Paris (LCMCP), UMR CNRS 7574, 4 place Jussieu, Paris, F-75005, France

[b] Synchrotron SOLEIL, L'Orme des Merisiers Saint-Aubin, BP 48 91192 Gif-sur-Yvette Cedex, France

[c] Netherlands Organisation for Scientific Research (NWO), DUBBLE@ESRF BP CS40220, 38043 Grenoble, France

[d] ESRF – The European Synchrotron, CS40220, 38043 Grenoble, France

* Corresponding author:

Dr. Niki Baccile

E-mail address: niki.baccile@sorbonne-universite.fr

Phone: +33 1 44 27 56 77

Abstract

Low molecular weight (LMW) molecules of biological origin like microbial glycolipid biosurfactants can self-assemble in water, with tunable structure by a soft chemistry approach (pH, temperature, ionic strength). The unique structure of glycolipids give possible access to a wide variety of aqueous self-assembled structures, although highly unpredictable beforehand. The glycolipid presented here consists in a glucose group linked to a C18:1-cis fatty acid (G-C18:1) and produced by the fermentation of *S. bombicola* Δ*ugtB1*. Due to the carboxylic group of the fatty acid, the supramolecular self-assembly is pH dependent. In the pH range 5 – 7, G-C18:1 forms vesicles, while above pH 7, it forms a micellar phase. Adding a wide range of metal salts (ion radius ascending order : Al^{3+}, Fe^{3+}, Ni^{2+}, Mg^{2+}, Cu^{2+}, Zn^{2+}, Co^{2+}, Fe^{2+}, Cr^{2+}, Mn^{2+}, Au^{3+}, Ca^{2+}, Ag^{+}, Sr^{2+} and Ba^{2+}), the vesicle phase generally precipitates. Metal salts with complex speciation (Al^{3+}, Cu^{2+}, Co^{2+}, Fe^{2+}) added to the micellar phase drive the formation of wormlike gels, often observed for surfactants in water. On the contrary, free metal ions (Cr^{2+}, Mn^{2+}, Ca^{2+} and Ag^{+}) added to the same micellar phase unexpectedly drives the formation of hydrogels with fibrillar structure, generally observed for complex

amphiphiles (peptides, peptide-derivatives) but not for surfactants. Oscillatory rheology shows that the elastic properties vary between few tens of Pa up to 5 kPa for a given glucolipid concentration (3 wt%).

Introduction

Supramolecular metallogels receive nowadays a growing interest for their potential applications in many areas, like medicine, drug delivery, environmental remediation, catalysis, electronics.[1–3] The growing interest of this family of gels comes from both the stimuli-responsiveness of the supramolecular self-assembly, and the interesting properties of the metal complex.[4,5] The supramolecular self-assembly is generally driven by non-covalent interactions, like Van der Waals contributions, π-stacking in water and the entropic effect related to the release of water. These attractive forces are counterbalanced by repulsive interactions like electrostatic repulsions, hydration forces or steric hindrance. In the specific case of metallogels, metal-ligand coordination contribute to the self-assembly process.[6]

Metallogels have been described for a broad set of compounds, from low-molecular weight (LMW) gelators[7–9] to peptide amphiphiles[10–12] as well as a broad set of polymers.[13–17] Excluding polymer-based, metallogels from LMW compounds or peptide amphiphiles are generally constituted of an entangled network of semicrystalline fibers. In this regard, the other important class of amphiphiles, surfactants, rarely forms metallogels, of which the structure is broadly accepted as an entangled network of wormlike micelles.[18,19]

The present communication shows that a new class of biobased surfactants is able to form fibrous metallogels, thus behaving as LMW gelator or peptide amphiphiles rather than surfactants. Historically developed to replace petrochemical surfactants, biological amphiphiles, also known as biosurfactants, are produced by the fermentation process of yeasts or bacteria in the presence of sugar and fatty acids.[20,21] So far, a number of properties (detergents, emulsion stabilizers, depollution, antimicrobials) and potential domains of applications (food science, environmental remediation, cosmetics, agricultural science)[22–24] have been reported in the literature, with a particular interest for their self-assembly in solution and at interfaces.[25] Hydrogel formation,[26–29] effect of salt on self-assembly[30–33] and heavy metals removal[31,34–37] have been spuriously reported in the past few years within the context of developing soft materials or tackling depollution. However, a lot of work has still

to be done and there has been no evidence of the potential effect of cations on the formation of biosurfactant hydrogels. The effect of cations on biosurfactants has not been much studied. Micellar solutions of sophorolipids seem to be poorly affected by mono and divalent cations,[30] just as rhamnolipids,[32] and surfactin, except, in the latter, for Ca^{2+} and Ba^{2+}, which do provoke a structural change, although not well identified so far.[33]

The biosurfactant used in this work, G-C18:1, is a glucolipid containing a glucose headgroup (G) linked to a fatty acid (C18:1) and produced by the fermentation of *S. bombicola ΔugtB1*.[38] Due to the carboxylic group of the fatty acid, the supramolecular self-assembly is pH dependent at concentrations below 5 wt%: below pH 7, G-C18:1 behaves as a lipid and it forms vesicles and lamellae, while above pH 7 it behaves as a surfactant and it forms a micellar phase.[39] Addition of ions to the vesicle phase drives precipitation, while addition of alkali earth and transition metal cations to the micellar phase drives hydrogel formation. Al^{3+}, Cu^{2+}, Co^{2+}, Fe^{2+}, Cr^{2+}, Mn^{2+}, Ca^{2+} and Ag^{+} induce gelation with elastic moduli in the kPa range, as probed by oscillatory rheology, while Fe^{3+}, Ni^{2+}, Mg^{2+}, Zn^{2+}, Au^{3+}, Sr^{2+}, Ba^{2+} induce aggregation and precipitation. A combination of small-angle X-ray scattering (SAXS) and cryo-transmission electron microscopy (cryo-TEM) show that all metallogels have a filamentous network. Al^{3+}, Cu^{2+}, Co^{2+} and Fe^{2+} promote the formation of wormlike gels. This is in agreement with several studies showing gelification of anionic sulfate surfactants by multivalent ions, like Al^{3+}.[18,19] On the other hand, Cr^{2+}, Mn^{2+}, Ca^{2+} and Ag^{+} unexpectedly promote fibrillation, a phenomenon which is never observed for metal-surfactant systems but rather for other amphiphiles (peptide amphiphiles or LMW gelators).[7–12] Concerning biosurfactants, fibrillation has only been observed for sophorolipids and cellobioselipids under acidic conditions, and never in the presence of salt.[25]

This work does not only show the metallogel properties of a glycolipid biosurfactant, thus broadening the perspectives of applications for this class of bio-based molecules. It also shows the richness and complexity of their unique phase behaviour, which can span, within a contained pH range and type of cation, from micelles to single- and multilamellar wall vesicles but also fibers, setting this unique molecule at the cross-road of lipids, surfactants and LMW gelators.[40]

Materials and methods

Chemicals. The biosurfactant used here is purchased from the Bio Base Europe Pilot Plant, Gent, Belgium, lot N° APS F06/F07, Inv96/98/99 and used as such. The monounsaturated

glucolipid G-C18:1 (M_w = 460 g.mol^{-1}) contains a β-D-glucose unit covalently linked to oleic acid. The molecule is obtained by fermentation from of the yeast *Starmerella bombicola (ΔugtB1)* according the protocol given before.[38] The salts, NaCl, $AgNO_3$, $FeCl_2.4H_2O$, $MnCl_2$, $CrCl_2$, $CuCl_2$, $NiCl_2.6H_2O$ and $FeCl_3.6H_2O$ are purchased from Sigma Aldrich, $CoCl_2.6H_2O$ come from Fluka, $ZnCl_2$ come from Strem chemical, $CaCl_2$ is purchased from VWR and $AlCl_3.6H_2O$ come from Across Organics. NaOH (≥98wt% pellets) is purchased from Sigma Aldrich and a liquid 35wt% HCl is purchased from VWR.

Sample preparation. The glucolipid G-C18:1 (concentrations given in the main text) is dispersed in milli-Q water by vortexing and sonication. The pH 8 is reached by adding few µL of concentrated NaOH (5 M). Exact pH is refined with µL-amount of NaOH solutions of 1 M, 0.5 M and 0.1 M. Salts solution are prepared at 1 M and added to the G-C18:1 solution so to reach the chosen cation-to-G-C18:1 ratio, provided in the main text. Typically, for a total 1 mL volume, 62.5 µL of AgNO3 (1 M), or 40 µL of CaCl2 (1 M), are added to the complementary volume of 3 wt% G-C18:1 in order to reach [AgNO3]/[G-C18:1] = 1.0 and [CaCl2]/[G-C18:1] = 0.6, respectively. A similar procedure is employed for all cations. Immediately after the cation addition, the solution is stirred during about 30 s. Samples studied here are prepared between few minutes and one day before any measurement. Throughout the text, the salt-to-lipid ratios are provided either in the form cation-to-G-C18:1 ratio, $[M^{z+}]/[G\text{-}C18:1]$, with $M^{z+}= Ca^{2+}$, Al^{3+}, Fe^{2+}… or, when relevant, in the form positive-to-negative charge ratio, $[X^+]/[G\text{-}C18:1]$, with $[X^+]= 2[Ca^{2+}]$, $3[Al^{3+}]$, $2[Fe^{2+}]$…, assuming that at pH> 8, all G-C18:1 molecules bear a negative charge related to the ionized carboxylic acid.

Small angle X-ray scattering (SAXS). SAXS experiments have been performed on SWING beamline at the SOLEIL synchrotron, Saint-Aubain, France and BM29, BM26 beamline at the ESRF synchrotron, Grenoble, France. All SAXS experiments are performed using hydrogel and solutions samples prepared at room temperature and analyzed into 1.5 mm quartz capillaries. Samples are manually injected into the capillary using a 1.0 mL syringe.

The Swing beamline is used with an energy of E = 12 keV and a fixed sample-to-detector (Eiger 4M - Dectris) distance of 2.005 m. The BM29 beamline is used with an energy of E = 12.5 KeV and a sample-to-detector distance of 2.83 m. The BM26 beamline is used with an energy of E = 12 keV and a sample-to-detector distance of 2.6 m. q is the wave vector, with $q = 4\pi/\lambda \sin(\theta)$, 2θ corresponding to the scattering angle and λ the wavelength. The q-range is

calibrated between ~ 0.05 < q / nm^{-1} < ~ 5, using the standard silver behenate calibrant (d(100) = 58.38 Å); raw data obtained on the 2D detector are integrated azimuthally using the in-house software provided at the beamline and thus to obtain the typical scattered intensity I(q) profile. Absolute intensity units are determined by measuring the scattering signal of water (I(q=0) = 0.0163 cm^{-1}).

Cations/solutions used	**Beamline**	**Synchrotron**	**Proposal N°**
Ca^{2+}, Fe^{2+}, Al^{3+}	SWING	Soleil	20201747
Cu^{2+}, Ag^{+}, Na^{+}, G-C18:1 alone	BM29	ESRF	MX 2311
Mn^{2+}, Cr^{2+}, Co^{2+}, Zn^{2+}, Ni^{2+}, Fe^{3+}	BM26	ESRF	SC-5125

Cryogenic-transmission electron microscopy (Cryo-TEM). Pictures are recorded on an FEI Tecnai 120 twin microscope operating at 120 kV with an Orius 1000 CCD numeric camera. The sample holder is a Gatan Cryo holder (Gatan 626DH, Gatan). Digital Micrograph software is used for image acquisition. Cryo-fixation is done with low dose on a homemade cryo-fixation device. The solutions are deposited on a glow-discharged holey carbon coated TEM nikel grid (Quantifoil R2/2, Germany). Excess solution is removed and the grid is immediately plunged into liquid ethane at -180°C before transferring them into liquid nitrogen. All grids are kept at liquid nitrogen temperature throughout all experimentation. Cryo-TEM images are treated and analyzed using Fiji software, available free of charge at the developer's web site.

Rheology. A MCR 302 rheometer (Anton Paar, Graz, Austria) is used with cone-plate geometry (Ø: 50 mm) at a regulated temperature of 25°C. A solvent trap with water is used to minimize evaporation. ~ 0.5mL of gel is loaded on the center of the plate using a spatula to prevent trapped bubbles, then the excess is removed. All the samples are made one day ±2h before the measurement except the Co^{2+}-containing G-C18:1 hydrogel, which is made 30 min before measurement. Experiments are performed in the linear viscoelastic regime (LVER). Value of the pseudo-equilibrium G' is taken after 5 min of oscillatory measurement at 1 Hz and low strain γ, one order of magnitude lower than the critical strain at 0.1%. Frequency sweep experiments are performed at a strain of 0.1%.

Results

The pH-dependent phase behaviour of G-C18:1 has been reported in previous work.[39,41] In the range between pH 8 and pH 6, G-C18:1 undergoes a micelle-to-vesicle transition, with a coexistence of wormlike micelles and flat open membranes around pH 7. We have qualitatively observed that addition of salt below pH 6, in the vesicle region, induces precipitation, most likely due to compensation of the negative charges of the lipid and formation of multilamellar structures, as found for many other systems.[42] However, upon adding NaCl in the micellar region above pH 7, when G-C18:1 behaves as a surfactant, the solution stays clear (images in Figure 1), without any remarkable effects on the macro scale. SAXS experiments in Figure 1 performed on an aqueous solution of G-C18:1 at room temperature and pH 8 confirms that NaCl does not significantly perturb the morphology of the self-assembled G-C18:1 structures. In the absence of NaCl, the SAXS profile (red) is characterized by a -2 dependence of the scattered intensity with q (in log-log scale), a broad hump centered at 0.7 nm^{-1} and an oscillation above 1.5 nm^{-1}. These features are typical of large flat 2D structures (-2 slope) coexisting with micellar aggregates undergoing repulsive electrostatic interaction (hump).[43] These data are in full agreement with previous results describing the micelle-to-vesicle transition between pH 8 and 6.[39,41] By adding NaCl to this system, one can observe the following: 1) in the low-q and high-q regions, the scattering profile is not sensibly affected from a ratio $[Na^+]$/[G-C18:1] 0.2 to 9.2, indicating that all solutions are characterized by a micellar phase coexisting with transitory flat structures; 2) in the mid-q region, the broad hump is less pronounced, and it flattens out by increasing the salt content; this is typical of the charge-screening effect of Na^+, as reported for other glycolipid biosurfactants.[30] The very good stability of the micellar phase at large ionic strength could be explained by the bolaform shape of the molecule, of which the hydrophilic extremities are localized on the micellar outer shell, as reported for another biosurfactant bola-amphiphile.[44] The mild chao/kosmotropic character of both Na^+ and Cl^- could also explain the stability of the micellar phase.[45] Literature work suggests that sphere-to-rod transitions are promoted by adding electrolytes to negatively-charged micelles,[19,46] but it has also been shown that this phenomenon depends on the concentration of salt.[47] Simple charge-screening effects without impacting the micellar morphology were also previously reported on sophorolipid[30] and rhamnolipid[32] biosurfactants in the presence of Na^+ and Ca^{2+}.

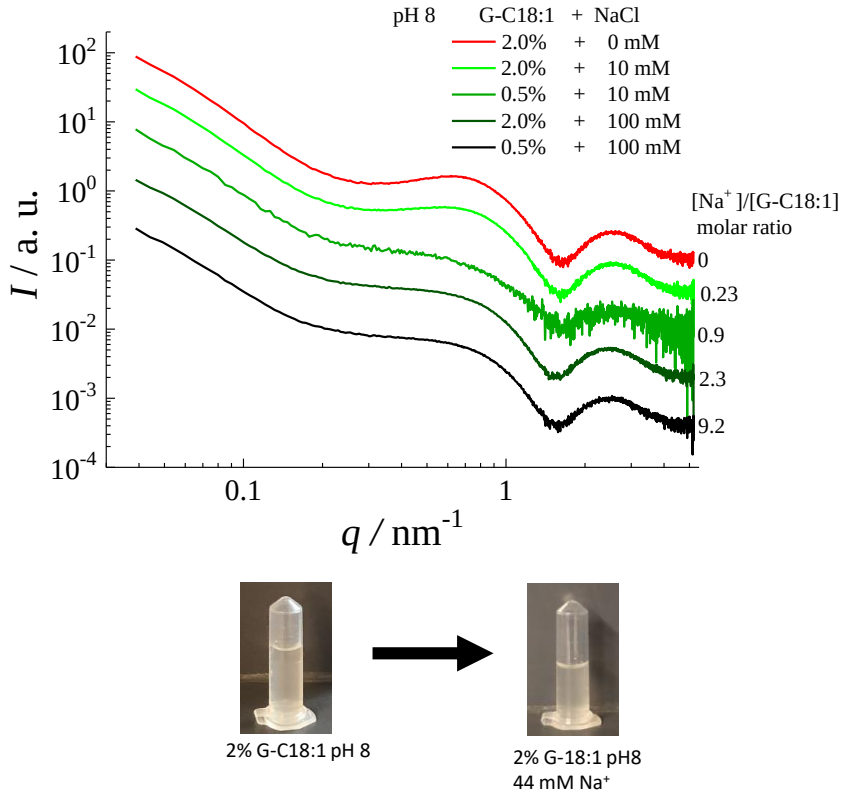

Figure 1 – SAXS spectra of a G-C18:1 microbial glucolipid solution at pH 8 and room temperature with a ratio [Na^+]:[G-C18:1] varying from 0 to 9. Concentration of G-C18:1 and NaCl are given in the figure. Concentration of 0.5 wt% and 2.0 wt% of G-C18:1 (Mw= 460 g/mol) corresponds to 10.8 and 43.5 mM, respectively.

A strong impact on both the macroscopic state of the samples and the corresponding SAXS profiles (Figure 2) is observed upon addition of multivalent cations to a G-C18:1 micellar solution at pH 8. The control profile of the salt-free G-C18:1 liquid solution at the same pH is shown by the black line in Figure 2b for convenience.

Mn^{2+}, Cr^{2+}, Ag^{+}, Ca^{2+}, Co^{2+}, Cu^{2+}, Al^{3+} and Fe^{2+} induce gelation with a sparse degree of gelling kinetics, ranging from immediate for Ca^{2+} or Ag^{+} to several hours for Fe^{2+} or Mn^{2+}. The corresponding typical photographical picture and SAXS profiles are given in Figure 2a. On the contrary, Fe^{3+}, Au^{3+}, Mg^{2+}, Sr^{2+}, Ba^{2+}, Ni^{2+} and Zn^{2+}, of which the typical image and selected SAXS profiles are given in Figure 2b, promote aggregation and/or precipitation, with no tendency to form stable gels. Compared to the control, all samples display very different profiles in the entire q-range, demonstrating a complete morphological and structural change of the initial micelles. For the samples, where a precipitate forms, one can distinguish two type of SAXS patterns. Fe^{3+} and Zn^{2+} (Figure 2b) show three peaks with a 1:2:3 ratio ($q_{(001)}$= 1.17 nm^{-1}), indicative of a lamellar order, and a low-q slope between -3.4 and -4, altogether

indicating the presence of lamellar precipitates with a fractal surface.[48] Ni^{2+} is on the contrary characterized by a nice high-q oscillation and a low-q slope of -1.9, probably representative of colloidal structures having a flat cross-section.[43] To note that for Au^{3+}, Mg^{2+}, Sr^{2+}, Ba^{2+} cations, the strong aggregation prevents the SAXS measurement in solution. These samples were not investigated further.

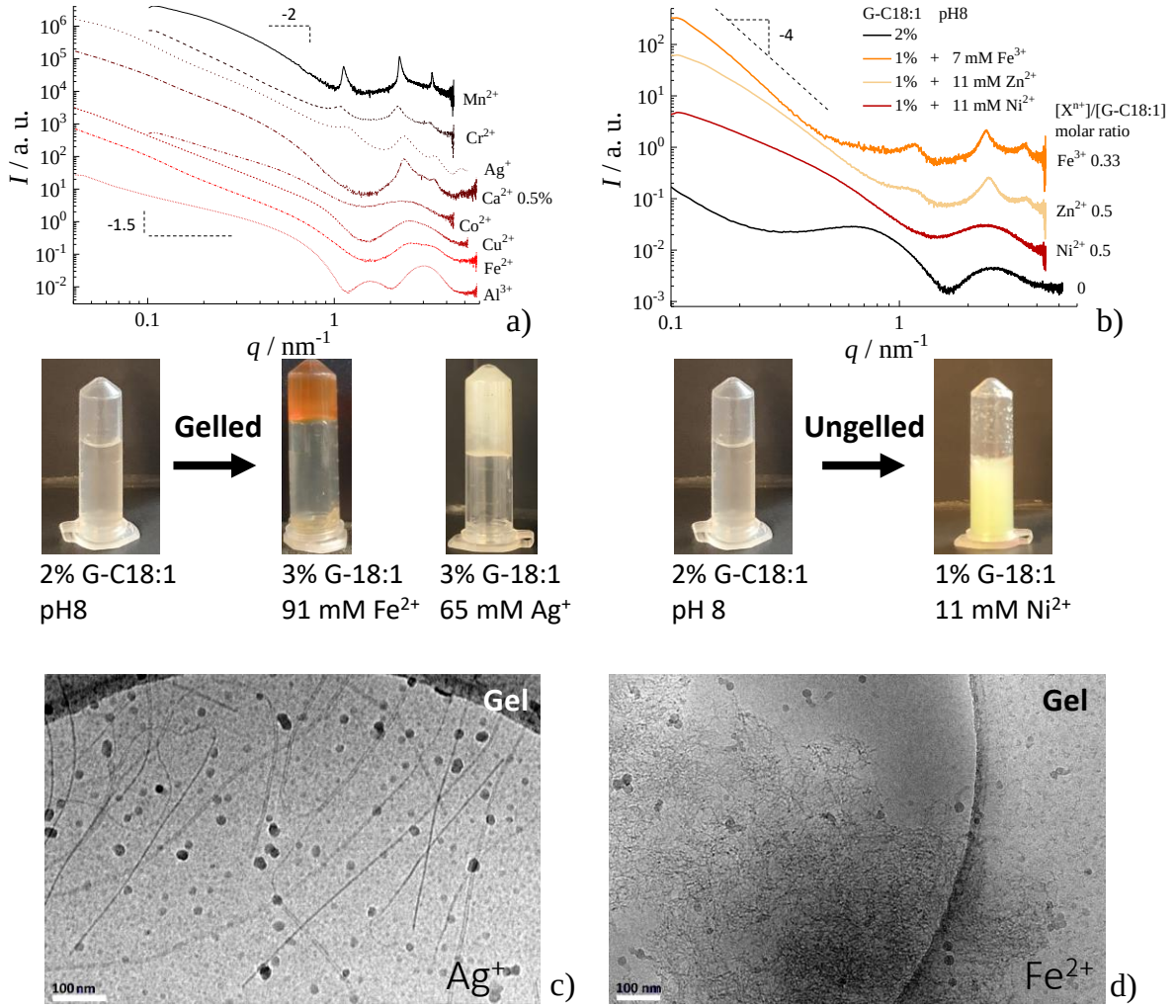

Figure 2 – SAXS profiles of a) G-C18:1 solution initially at pH 8 (0.5 < C / wt% < 3) gelled by Mn^{2+}, Cr^{2+}, Ag^{+}, Ca^{2+}, Co^{2+}, Cu^{2+} or Al^{3+} ([ion]:[G-C18:1] molar ratio vary between 0.5 and 1.5) and b) G-C18:1 aggregates containing Fe^{3+}, Ni^{2+} and Zn^{2+}. Image of the reverse tube illustrate a typical gel in a) and aggregation in b). Cryo TEM images of G-C18:1 solution at 0.5% (10.8 mM) containing c) Ag^{+} at 10.8 mM and d) Fe^{2+} at 16 mM. In c,d), the dense, contrasted, spheroidal aggregates are attributed to artifacts due to freezing.

Metallogels in Figure 2a also display two families of SAXS patterns. Mn^{2+}, Cr^{2+}, Ag^{+} and Ca^{2+} gels are characterized by well-defined diffraction peaks, most of which are in the ratio 1:2:3 ($q_{(001)}$= 1.15 nm^{-1} on average) and a low-q slope contained between -2 and -2.8.

Co^{2+}, Cu^{2+}, Fe^{2+} and Al^{3+}, on the contrary, display one or two high-q oscillations and a low-q slope between -1.5 (Al^{3+}, Co^{2+}) and -2.2 (Cu^{2+}, Fe^{2+}). The broad variation in terms of low-q slopes makes the morphological and structural interpretation not obvious. One should recall that the dependency of log(I)-log(q) at low scattering vectors (slope) identifies either a specific shape (-1: rod, -2: plane)[43] or mass (-1 / -3) and surface (-3 / -4) fractals.[48] For the systems showing a lamellar order, the first correlation peak corresponds to a repeating distance of about 5.5 ± 0.3 nm, twice the molecular size of G-C18:1, considering the Tanford formula for the alkyl chain.[39,41,49]

On the basis of SAXS alone, one could assign most of the gel structures to a lamellar phase and class them with the rare family of lamellar hydrogels.[50] This could not be so surprising, because the glycolipid G-C18:0, the saturated analogue of G-C18:1, was reported to form lamellar hydrogels at room temperature.[51] However, SAXS alone is not sufficient to elucidate the structure and complementary techniques, like microscopy, should be employed. Cryo-TEM images (Figure 2c,d) collected on selected diluted metallogels, Ag^{+} and Fe^{2+}, respectively representative of the two families of SAXS profiles, rather support the formation of thread-like structures, instead of lamellar ones. Cryo-TEM of Ag^{+} sample shows the presence of nanofibers (Figure 2c), while the Fe^{2+} sample (Figure 2d) shows an aggregated fibrous network. In this regard, the SAXS patterns in Figure 2a should rather be associated to flat belts, when the slope is close to -2 (e.g., Ag^{+}, Ca^{2+}),[52] or to a fractal network of aggregated fibers when the slope varies between -1.6 and -2.2 (e.g., Al^{3+}, Fe^{2+}). In the latter, the lack of structural peaks and the type of oscillation of the form factor above 1 nm^{-1} suggest that the cross-section of the individual threads is micellar worm-like[53] rather than flat and crystalline. Surprisingly, neither lamellae nor vesicles, as one would reasonably expect for G-C18:1 considering previous data,[39,41] are observed, making this molecule unique.[40]

As a short summary, on the basis of microscopy and SAXS, G-C18:1 metallogels from Mn^{2+}, Cr^{2+}, Ag^{+} and Ca^{2+} fall in the category of self-assembled fiber networks (SAFiN), where G-C18:1 behaves as LMW gelator or amphiphile peptide.[7–12] Meanwhile, Co^{2+}, Cu^{2+}, Fe^{2+} and Al^{3+} rather induce a sphere-to-wormlike transition, as classically found for anionic surfactant-multivalent ion systems,[18,19] and seldom displaying some viscoelasticity.[18,19] Deeper structural insights in the structure of the fibers and in the mechanisms of phase transitions are reported by us elsewhere.[54,55]

The elastic properties of the metallogels are probed by oscillatory rheometry. The metallogels are prepared by adding few µL of the cation solution (1 M, Ag^{+}, Co^{2+}, Al^{3+}, Cu^{2+}, Ca^{2+}, and Cr^{2+}) in 1 mL of G-C18:1 solution at 3 wt% at basic pH 8 (Figure 3a). The ion-to-

G-C18:1 ratio is always controlled. The solution is immediately stirred few seconds after addition of the cation. pH drops some systems, e.g. Co^{2+} and Cr^{2+}, but this is not systematic, as discussed later. The elastic properties are measured about 24 h after the cation addition, except for Co^{2+} where the strong syneresis imposes a measurement few minutes after the preparation.

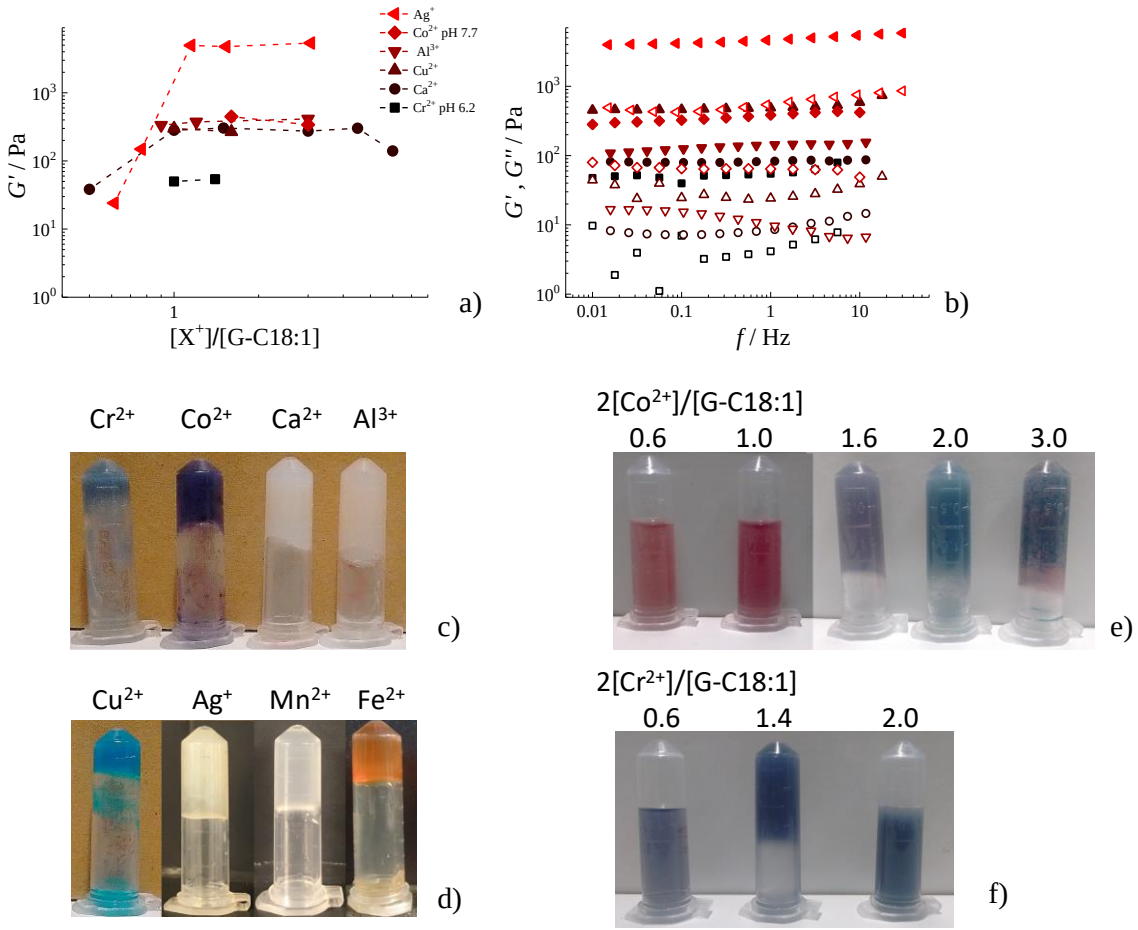

Figure 3 - a) Elastic modulus of G-C18:1 (C= 3 wt%) metallogels as a function of the charge-normalized cation molar concentration for different salts. For Co^{2+} and Cr^{2+}, the pH refers to the final manually-adjusted pH, required to obtain a gel. b) Frequency sweep measurement of the corresponding gel systems in a) at the plateau. c,d) Typical images of G-C18:1 (C= 3 wt%) metallogels after about 24 h from preparation. e,f) Co^{2+} and Cr^{2+} based G-C18:1 (C= 3 wt%) metallogel freshly prepared at pH 7.7 and 6.2 for different ion-to-glucolipid charge ratio.

A frequency sweep measurement is systematically performed (Figure 3b). For all cations, the weak frequency-dependence and the loss modulus, G'', being about one order of magnitude lower than the elastic modulus, G', demonstrates the solid-like behaviour of the gel. The elastic modulus is taken on the plateau of the frequency sweep experiments (Figure 3b) for different ion-to-G-C18:1 ratio. However, for a matter of convenience, we report the

charge ratio, which is determined in relationship to the valence of the cation. For $[Ag^+]$, the charge content corresponds to $[X^+] \equiv [Ag^+]$, but for $[Co^{2+}]$ or $[Al^{3+}]$, $[X^+]= 2[Co^{2+}]$ or $3[Al^{3+}]$, respectively. Considering that each G-C18:1 carries a COOH group and reasonably assuming that at pH 8 all carboxylic acids are in the form of COO^-, one can measure the critical charge ratio $[X^+]/[G\text{-}C18:1]$ required to obtain a gel. The values of G' against $[X^+]/[G\text{-}C18:1]$ for each metallogel are reported in Figure 3a, while the critical ratio at which metallogels form are indicated in Table 1. Figure 3c,d illustrate the typical macroscopic look of G-C18:1 metallogels prepared with various cations.

Table 1 – List of cations inducing gelation of a G-C18:1 solution. Here, the concentration of G-C18:1 is 3 wt% at a pH= 8. The charge ratio indicates the minimal value, above which the gel strength doesn't increase anymore (Figure 3a). Additional information is given on final pH after gelation, typical elastic modulus, gelation and stability in time, color and general remarks.

Cations	$[X^+]/[G\text{-}C18:1]$	G' / Pa	Final pH after cation addition ± 0.1	Gelation time	Syneresis process	Color	Remarks
Ag^+	1.0	5000	8 ± 1	Seconds	Day	White, slightly translucent	Light sensititve
Co^{2+}	1.6	400	6.8	Second	Hours	acidic pH: transparent pink solution pH 7.7: opaque blue gel	Immediate gelation after basification at pH 7.7
Al^{3+}	0.9	375	3 ± 0.5	Minutes	Days	White opaque	
Cu^{2+}	1.0	280	5.1	Seconds	Days	Blue, translucent	
Ca^{2+}	1.0	80 - 300	8	Seconds to minutes	Week	White opaque	
Cr^{2+}	1.0	50	4.8	Seconds	A day	acidic pH: opaque grey pH 6.3: opaque navy blue	Immediate gelation after basification at pH 6.3
Mn^{2+}	/		6.1	Day	Week	white translucent	
Fe^{2+}	/		4 ± 0.5	Hours	Days	Orange translucent	Gentle mixing to homogeneously gel

Cations inducing gelation are presented by the descending order of the elastic modulus in Table 1. The charge ratio at which metallogels form is close to 1 for all cations, thus suggesting the crucial contribution of the charge. However, the initial morphology at which fibrillation occurs is also crucial. Indeed, the negatively-charged micellar phase of G-C18:1 (pH > 7) can be shifted to a gel phase, differently than the vesicle phase (pH 5 – 7), which precipitates immediately after addition of salt. The effect of the initial pH is particularly important and it has been tested on three systems, Ca^{2+}, Fe^{2+} and Al^{3+} (Figure 4). Whichever the cation, the elastic moduli at pseudo equilibrium G'_0 (Figure 4a) shows a drastic increase

between pH 7 and 8, indicating that abundancy of the micellar phase above pH 7 is an important requirement to obtain a gel. Frequency sweep experiments (Figure 4d) are shown only for the calcium gel, which is representative of the gels characterized here. At pH 7, the frequency dependency of G' shows a fluid, rather than a solid-like, structure if compared to higher pH. The critical strain, γ_c, related to the strain required to break the network, is determined for the calcium gel (Figure 4c) by the intersection of the linear fits below and above the LVER. At pH 7, the linear viscoelastic domain doesn't exist and associated γ_c doesn't correspond with the stiffness of the gel. Between pH 8 and 10 (Figure 4b), the critical strain is constant.

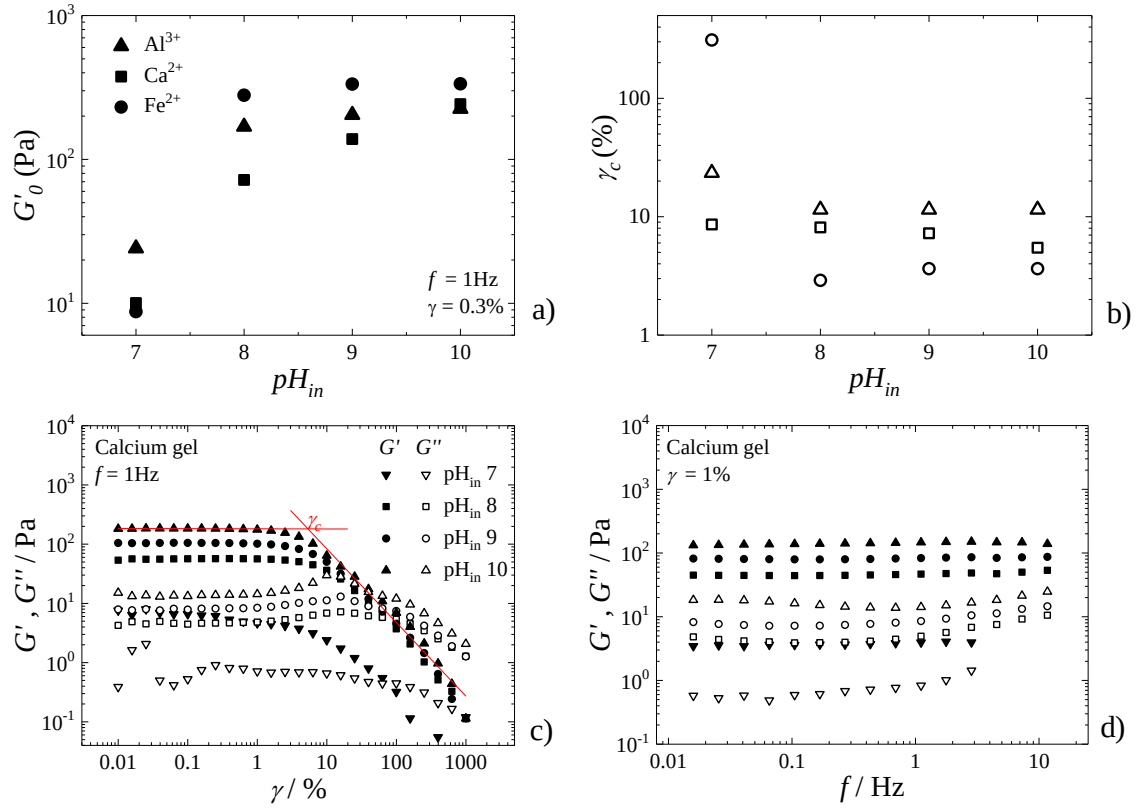

Figure 4 - a) Elastic moduli at pseudo equilibrium, G'_0 and b) critical strain, γ_c, of G-C18:1 hydrogels containing Ca^{2+} (square), Al^{3+} (triangle) or Fe^{2+} (circle) as a function of the initial pH, pH_{in}, of the G-C18:1 solution ($C_{G\text{-}C18:1}$= 3 wt%) at the molar ratio $[Al^{3+}]/[G\text{-}C18:1]$ = 0.38, $[Ca^{2+}]/[G\text{-}C18:1]$= 0.61, and $[Fe^{2+}]/[G\text{-}C18:1]$ = 1.4. c) Strain sweep experiment for calcium hydrogel, critical strain γ_c correspond to intersection of fit at linear viscoelastic domain and high strain. d) Frequency sweep experiment for calcium gel, curves shapes are representative of aluminium and iron derived hydrogels.

If the ion-to-lipid ratio and pH are crucial to obtain a gel, the nature of the ion is just as important, as shown by the lack of phase transition even up to the ion-to-surfactant ratio of 9:1 when Na^+ is added to the micellar phase. This suggests the presence of interactions like

complexation and coordination, as found for many other anionic surfactants mixed with multivalent cations.[19,46,56–59] The broad set of data in our possession (Figure 3 and Ref.[54,55,60]) shows that self-assembly and gelling occurs at a well-defined ion-to-surfactant molar ratio. Rheological experiments tend to show that metallogels form when the ion-to-glucolipid charge ratio is close to 1, suggesting that charge stoichiometry is crucial. However, isothermal titration calorimetry (ITC) experiments[55] rather show a 1:2 ion-to-glucolipid ratio, for both Ag^{+} and Ca^{2+} derived gels. Considering the difference valence of silver and calcium, ITC tends to show a complexation effect for silver and a double charge-screening and complexation mechanism for calcium. More details about the structure and mechanism of fiber formation will be given elsewhere.[54,55]

Table 2 –List of cations, which do not induce gelation of G-C18:1 in water.

Cations	$[M^{z+}]/[G\text{-}C18:1]$	Color	Homogeneity	Remarks
Zn^{2+}	0.44 - 0.53	White translucent	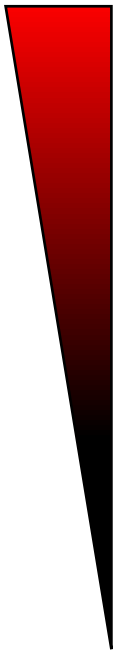	Viscosity increase
	0.53 - 1.8	White opaque		Fluid
Fe^{3+}	0 - 1.36	Orange opaque		Fluid
Ni^{2+}	1	Green opaque		After basification at pH 7.7 a gel is formed during few minutes, then a phase separation occurs between aggregates and turbid solution.
Au^{3+}	0.04 - 1.5	Yellow transparent After one day : black aggregates		Initially yellow fluid. After one day black millimeter range aggregates in transparent solution.
Mg^{2+}	1.7 - 7.7	White turbid		Liquid phase separation, (very viscous dense phase against transparent light phase).
Sr^{2+}	0.13 - 12.5	Orange aggregates		Aggregates formed at a ratio ≤ 0.5.
Ba^{2+}	0.01 - 12.5	Orange aggregates		No soluble

When other divalent (Zn^{2+}, Ni^{2+}, Mg^{2+}, Sr^{2+}, Ba^{2+}) and trivalent (Fe^{3+}, Au^{3+}) cations are added to the G-C18:1 solution, the initial micellar structure changes into aggregated threads, rather looking like giant micelles than fibers. The structure is poorly hydrated, insufficient to retain water and to form a gel (Table 2). For divalent alkali earth metals, Mg^{2+} induces phase separation in the state of a viscous liquid, while Sr^{2+} and Ba^{2+} are highly

reactive, immediately generating an aggregated precipitate. In the alkaline earth series, while only Ca^{2+} induces the formation of a homogenous and stable gel.

Discussion

Metallogels are generally reported for polymers, LMW and peptide-based amphiphiles,[7–17] more rarely for anionic surfactants,[18,19] and never for biosurfactants, of which the interaction with cations has only been described within the context of depollution and impact on micellar morphology.[25,31,34,61,62] According to Table S 1, where a broader list of references is provided, mono-, di- and trivalent cations have been largely explored. Without any doubt, Ca^{2+} is probably the most popular element (30% of all entries, Table S 1), followed by Al^{3+} (23%) and transition metal ions like copper, cobalt, iron, zinc, each representing between 10% and 15% of the entries. The great majority of literature studies exploring the interactions between metal ions and amphiphiles, or polymers, generally consider Coulombic or metal-ligand interactions between the negatively-charged group (sulfate or carboxylate) and the free ion form of the metal ions. However, in water, this assumption is mainly (although not exclusively) correct for alkaline and alkali earth cations at pH below about 10-11. A more general mechanism cannot disregard the well-known hydroxylation process of cations, which depends on the type of metal ion (radius, polarizability, eletronegativity) and pH.

All cations presented in Table 1 undergo the well-known hydroxylation reaction in water:[63]

$$xM^{z+} + yH_2O \rightleftharpoons M_x(OH)_y^{(xz-y)+} + yH^+$$

This reaction releases hydronium ions, thus strongly influencing the solution pH, and it is extremely sensitive to pH itself. Free metal ions are abundant at acidic pH, while hydroxo complexes are abundant at basic pH. However, the notion of acid and base are relative and the actual pH, at which free ions and hydroxo species are stable, depends on the chemical nature of the ion. Species-pH plots are known as speciation diagrams and they are reported for practically all elements.[63] For this reason, speaking of metal-ligand interactions in an indiscriminate way is not correct. Alkali metal cations are found in the form of free ions in water at pH between 5 and 8, at which most of the studies reported in Table S 1 are presumably performed. In this case, the assumption of metal-ligand interactions between amphiphiles and cations are reasonable. This may not the case for most studies performed on transition metal cations, which display complex speciation diagrams between pH 4 and 10.

Multiple hydroxo species, each having a different charge, generally coexist at the same time.[63,64] Each species can not only undergo Coulombic interactions with amphiphiles, but specific metal-hydroxo-ligand complexes could potentially form,[65] making the complete understanding more complex than expected. Out of the literature survey performed in Table S 1, less than 20% of the entries involving work with transition metal does mention speciation, and only one considers the possibility of interactions between the metal hydroxo species and the amphiphile.[66] In a similar way, little concern is given to the solution pH, which not only becomes more acidic when transition metals are introduced in solution, but it has a crucial impact on the number of coexisting species.

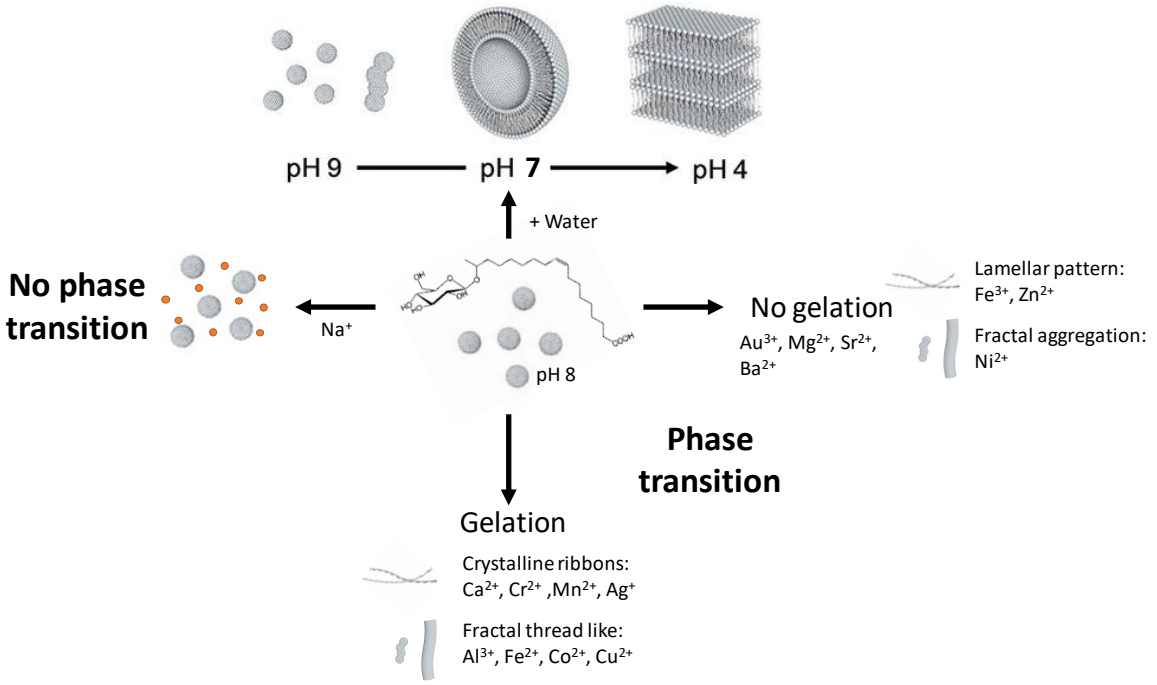

Figure 5 – Schematic representation of the self-assembly of G-C18:1 microbial glycolipid at room temperature in water as a function of pH and in the presence of ions at pH ≥ 8. For a broader insight of the phase behavior of G-C18:1 under diluted conditions in water, refer to ref. [40]**.**

The present work shows that microbial glycolipid G-C18:1 has metallo-responsive properties, similar to many other amphiphiles in the literature (Table S 1). The ability of G-C18:1 to form metallogels occurs with a number of both alkaline earth and transition metal ions (Table 1), also in agreement with many other amphiphiles (Table S 1). Metal-induced gelation adds further complexity to the phase diagram of G-C18:1.[40] Top of Figure 5 gives an illustration of the metal-free, pH-dependant self-assembly of G-C18:1 in water. G-C18:1 forms morphologies with high curvature, micelles, when the carboxylic acid is ionized, and low-curvature membranes upon partial and complete neutralization.[39] Similarly to other

literature studies,[42] cations induce precipitation of multilamellar structures when added to the vesicle phase. However, except for Na^+, wormlike and fibrillar objects, possibly followed by a sol-gel transition, form when cations are added in the micellar region of the phase diagram, when G-C18:1 is fully ionized. May them be wormlike micelles or fibers, each of these phases enrich the phase diagram of G-C18:1, making this molecule unique, not only compared to any other known biosurfactant,[25] but also to many other amphiphiles, including LMW gelators, peptide-based or surfactants (Tables S 1). This aspect was specifically discussed in Ref. [40]

All cations employed in this work, except Na^+, stimulate a sol-to-gel transition of G-C18:1. However, the fibers' morphology and structure vary according to the type of cation and gel formation is not systematic. Furthermore, from Figure 2, the structure of the gels may not be the same. These qualitative observations suggest that the interaction between the glucolipid and the ions are different from one ion to the other. Two main interactions could occur, charge screening and complexation. According to cryo-TEM and SAXS, G-C18:1 forms either fibers or wormlike micelles. The former is shown in Figure 2c and characterized mainly by a long-range lamellar order in the hydrate state (Figure 2a,c, e.g., Cr^{2+}, Mn^{2+}, Ca^+, Ag^+), while the latter is shown in Figure 2d and characterized by a scattering profile more often observed for wormlike micelles (Figure 2a,c, e.g., Ni^{2+}, Cu^{2+}, Co^{2+}, etc…). Table 3 summarizes the known aqueous species of the cations used in this study, as well as their effect on the structure and physical state of G-C18:1.

Table 3 – Summary of the structural and physicochemical properties of metallogels composed of G-C18:1 microbial glucolipid found in this work. Properties of cations: expected colour, coordination, speciation form and ionic radii in aqueous solution.[63,67,68] **Oh: octahedron; *d*Oh: distorted octahedron; Th: tetrahedron; *d*Th: distorted tetrahedron; Lin: linear; SA: square antiprism. *Ox*: oxidized form. * Oxidation occurs.**

Cation	Gel	Morphology Structure	Final pH	Experimental color	Expected color	Coordination	Expected species at Final pH	Ionic Radius / Å
Mn^{2+}	YES	Lam	6.1	pale	pale pink	Oh	Mn^{2+}	0.86
Cr^{2+} *(*Ox* -> Cr^{3+})	YES	Lam	(4.8 →) 6.3	grey->blue	blue	Oh/Th	*Ox* -> Cr^{3+}: $Cr(OH)^{2+}$ $Cr_3(OH)_4{}^{5+}$ $Cr(OH)_2{}^{+}$	0.65
Ag^+	YES	(SAFIN) Lam	5	white	-	*d*Th/Lin	Ag^+	0.98
Ca^{2+}	YES	(SAFIN) Lam	6.8	white	-	SA	Ca^{2+}	1.12
Zn^{2+}	NO	Lam	-	White	-	Oh	Zn^{2+} $Zn_2(OH)^{3+}$	0.74

							$Zn(OH)^{+}$	
Fe^{3+}	NO	Lam	-	Orange	pale violet	Oh	$Fe(OH)^{2+}$ $Fe(OH)_2^{+}$ $Fe_3(OH)_4^{5+}$	0.66
Co^{2+}	YES	Micellar	(6.8 →) 7.7	pink--> blue	pink or blue	Oh or Th	Co^{2+} $Co(OH)^{+}$ $Co(OH)_2$	0.53
Cu^{2+}	YES	Micellar	5.1	light blue	light blue	Oh/*d*Oh	Cu^{2+} $Cu_2(OH)_2^{2+}$ $Cu(OH)^{+}$	0.62
Fe^{2+} *(*Ox*->Fe^{3+})	YES	Micellar	4	orange	green	Oh	Fe^{2+} [*Ox*->Fe^{3+}: $Fe(OH)^{2+}$, $Fe(OH)_2^{+}$, $Fe_3(OH)_4^{5+}$]	0.74
Al^{3+}	YES	Micellar	3	White	-	Oh	Al^{3+} Al_{13}	0.53
Ni^{2+}	NO	Micellar	-	Green	green	Oh	Ni^{2+} $Ni(OH)^{+}$	0.62

Although a comprehensive understanding of the effect of each specific cation on G-C18:1 is out of the scope of this work, one can observe some general trends, which help understanding the differences and similarities across the samples. Ag^{+} and Ca^{2+} form SAFIN gels with an unexpected lamellar association in the gel state and described in more detail elsewhere.[55] Mn^{2+} and Cr^{2+} gels show the same SAXS profile and, by analogy, one can conclude in the formation of similar SAFIN with lamellar order. Similar conclusions can be drawn for Zn^{2+} and Fe^{3+} samples, although they do not form gels. All other cations (Co^{2+}, Cu^{2+}, Fe^{2+}, Al^{3+} and Ni^{2+}) form micellar gels except Ni^{2+}.

SAFIN gels are systematically obtained in the pH range below 8 and mainly for those cations, which have larger radius and are known to be in their free ion form, according to their speciation.[63] Their strong affinity towards carboxylates[65] suggests the formation of coordination complexes. Interestingly, most of these ions prefer tetrahedral or linear coordination, rather than the most classical octahedral one. In the literature, cation-induced fibrillation and possible gelation is often observed for LMWG, peptides, or peptide derivatives, as summarized in Table S 1. However, in the case of G-C18:1, fibrillation occurs in its micellar phase, that is when it behaves as a surfactant. Exception made for specific (e.g., gemini) surfactants interacting with chiral organic counterions,[69] fibrillation of surfactants and lipids in the presence of metal ions is generally never observed (Table S 1). Free metal ions, like Ag^{+}, Ca^{2+} or Mn^{2+}, then switch the behaviour of G-C18:1 from surfactant-like to peptide- or LMWG-like. This effect, and fibrillation of G-C18:1 in general, is then quite unique.

Micellar gels of G-C18:1, on the contrary, are mainly observed for ions of smaller size and with a richer speciation in water at pH below 8. They are characterized by a classical octahedral coordination, most likely provided by hydroxyl and free water. Coordination by

the carboxylate or carboxylic acid (according to final pH) is not excluded, but the richness in the metal hydroxyde species and the kinetics of pH change[54] during gelation probably prevent the formation of one-single coordination complex involving G-C18:1. These results are more in line with the literature of anionic surfactants, which often form cylindrical[56–59] or wormlike[18,70] micelles in the presence of multivalent ions like Al^{3+}, among others (Table S 1). Wormlike gels are sometimes observed, although this is not a systematic behaviour.[18,19] Most of the literature studies invoke several classical mechanisms of interactions between the cations and the surfactant. However, except for some few example (ref to Table S 1),[18,66,70–74] most studies involving the use of transition metal ions do not consider speciation of the ion, making it unrealistic to satisfactorily describe the nature of the metal-ligand interactions.[66]

Some ions need specific comments. Fe^{2+} is soluble as a free ion in solution at pH below 8 and one could expect it to form a SAFIN gel, as found for Mn^{2+}. However, Fe^{2+} is known to be unstable in water and undergo prompt oxidation towards Fe^{3+}. This is confirmed by the orange, instead of green, colour of the Fe^{2+} gel (Table 3). Cr^{2+} is also unstable in water and it undergoes oxidation, as demonstrated by the blue colour in the gel, expected for Cr^{3+}. Speciation of Fe^{3+} and Cr^{3+} in solution is more complex than Mn^{2+} or Ag^{+}, and micellar gels should be expected. However, for Cr^{3+}, SAFIN gels are formed in the pH region between 5 and 7, upon increase of pH. According to the corresponding speciation diagram, free Cr^{3+} ions are the most abundant species in solution in this pH range. The tetrahedral coordination reported for Cr^{3+} could also explain the similarity with Mn^{2+} or Ag^{+} in terms of structure and properties of the corresponding gels. Variation of the coordination (octahedral or tetragonal) around the metal ion could explain the loss in the gel properties of chrome metallogels, which are stable only up to the ion-to-glucolipid ratio of 1.4 (Figure 3f). The importance of the coordination is also supposed for Co^{2+} metallogels. Figure 3e shows the images of Co^{2+} metallogels at pH 7.7 for different charge ratio, thus illustrating the color change. The colors of the gels vary from pink (ratio 0.6) to blue (ratio 2.0) for the sol and gel, respectively, whereas the blue color is characteristic of a tetrahedral complexation of Co^{2+}, while the pink color indicates an octahedral complex of Co^{2+} (Table 3). A similar evolution was also reported for triazole cobalt complexes.[75] Interestingly, by increasing the charge ratio up to 3 (Figure 3e), blue aggregates precipitate in a translucent pink environment, which would indicate the coexistence of two gel networks stabilized by two forms of Co^{2+}.

Despite the effort to rationalize the metal-induced gelation of the micellar phase of G-C18:1, one must acknowledge the lack of data to explain many observations. For instance, Zn^{2+} and Fe^{3+} do not form gels at all, similar as to Ni^{2+}, but have a lamellar and micellar

patterns, respectively. They all accommodate an octahedral arrangement of the ligands and display a complex speciation behaviour. The formation of neutral species, such as $Fe(OH)_3$, could explain the poor gel formation properties, although, a full understanding lacks at the moment.

Complete rationalization is unfortunately prevented by the concomitantly occurring combination of: acido-base reactions of both metal ions and G-C18:1, metal-ligand interactions, unknown for G-C18:1, and kinetics. Below, a non-exhaustive list of factors, which prevent a full understanding of this system.

1) *pH*. pH plays a crucial role in the gelling mechanism, as it affects, at the same time: the $COOH/COO^-$ ratio, the phase behaviour of G-C18:1 and the type and relative abundancy of metal species. Metallogel formation generally occurs upon addition of the metal ion to the G-C18:1 solution and pH generally drops. In some specific cases, gelation is triggered by a mild alkalinization of the solution (see Final pH column in Table 3), although this is not systematic. The way pH is controlled certainly deserves more attention, as found elsewhere for a fibrillating glycolipid biosurfactant,[27] although this is not the scope of this work.

2) *Chemistry of metal ions and ligand*. The reactivity of most metal ions has an impact on pH and consequently on the type and number of aqueous and hydroxy metal species. Meanwhile, pH variations strongly impacts the carboxylate-to-carboxylic ratio of the glucolipid and its phase behaviour. Here, the pH drops for most systems, often in an uncontrolled way and depending on time and the effect on gelation can sometimes be very important. When Co^{2+} or Cr^{2+} are added to the micellar solution of G-C18:1 at pH 8, the pH drops to about 6.8 and 4.8, respectively, and the solution is fluid. The sol-to-gel transition is promoted by increasing the pH to 7.7 and 6.3, respectively. On the contrary, Al^{3+} and Cu^{2+} systems, which also acidify the solution to pH 3 and 5.1 (Table 1), readily form gels. A tentative explanation to this opposite phenomenon is given in point N°7, below.

3) *Metal-ligand coordination*. The coordination geometry depends on the cation but for the same metal, different coordination geometries can occur. For instance, the geometry of Ag^+-carboxylate complexes is known to vary with the chemical environment[76] and Co^{2+} itself was shown to exist under two concomitant coordinations (pink, octahedral and blue tetrahedral, Figure 3e). In general, the aptitude of a metal to form complexes is hard to predict, as it strongly depends on the ligand's chemical structure, affinity, competition, etc...[65] The variation of affinity between divalent alkali earth metal and COO^- group is also known,[77] the hydration of self-assembled structure is also modulated according to the cation nature in despite of its charge by the water loving/hating effect of the cation.[78]

4) *The ion-to-ligand molar ratio*. This parameter is often related to the chemical nature of the ligand, especially if the latter can self-assemble into various structures,[79,80] as observed for Fmoc-based hydrogels, where the Fmoc : Zn^{2+} ratio produce at 2:1 a β-sheet structure, at 1:1 a helical ribbons while at 1:2 one can see a random coil structure.[81] In most systems studied in this work, gelation seems to occur at the stoichiometric charge ratio, although complementary ITC[55] and *in situ*[54] experiments show that the exact ratio may vary with the kinetics of the metal addition.

5) *Counterion and temperature*. Although not explored in this work, counterions and temperature can have a strong impact, as well.[82,83] For Ag^{+} - melamine complex, for instance, the gelation occurs only with NO_3^-, as NO_3^- could be sufficiently small to be entrapped during the crystallization process, allowing a sufficient layer of solvent entrapped through crystallization producing a gel.[79,80] In other systems, counterions could induce faster crystallization kinetics, which would hinder trapping of the solvent. It was found for bipyridine - Ag^{+} complex in the solid state, that increasing the counter anion size favors a self-assembly from helical to lamellar structure.[84] The temperature can also induce some change into the internal structure of the self-assembly, as shown for lanthanum-cholate complex, where the self-assembly change from helical fiber at 15°C to flat nano-ribbons at 50°C.[85]

6) *Kinetics*. The synergy between metal ion reactivity and ligand self-assembly have a strong, uncontrollable, impact on the gelation kinetics. Qualitative estimation of the gelation time shows a broad, cation-dependent, time-span, practically instantaneous for Cu^{2+} to about a day for Mn^{2+}, following this order: $Cu^{2+} < Ag^{+} < Ca^{2+} < Al^{3+} < Fe^{2+} < Mn^{2+}$. Gelation time for Co^{2+} and Cr^{2+} is also fast, occurring within less than a minute, however it cannot be directly compared to the other systems due to the difference in the protocol (increase in pH). Syneresis is generally observed for all gels, although at different time scales. Co^{2+} based hydrogel displays the strongest syneresis, which is visible after few hours, while that occurs only after one day or more for others cations (Table 1). Interestingly, in many cases, as that of Cu^{2+}, the water expulsed from the gel is colorless, thus suggesting a low amount of Cu^{2+} in solution and demonstrating its role in the fiber formation.

Kinetics could also play an important role in the acido-base reaction of both G-C18:1 and metals, as explained more precisely in 7b), below.

7) *Tentative overall mechanism*. When a given metal is introduced in the G-C18:1 solution, there are two possible mechanisms.

7a) If the metal exists as a free ion (e.g., Ca^{2+}, Ag^{+}), the pH of the solution is not immediately modified and G-C18:1 promptly interacts the metal center via a metal-COO^{-} coordination: SAFIN forms. The pH of this system may remain constant, as found through *in situ* experiments,[54] but we have experienced spurious pH drops over time from one experiment to the other. Spontaneous variations of pH after gelification do not seem to have an impact on the gel strength.

7b) If the metal exists as a complex mixture of species (e.g., for iron: $Fe(OH)^{2+}$, $Fe(OH)_2^{+}$ or $Fe_3(OH)_4^{5+}$), the pH of the solution becomes more acidic and the outcome may depend on the relative acido-base kinetics of the metal and G-C18:1 and the effective rate of pH change. If the acido-base reaction of G-C18:1 is slow (compared to the metal), the metal-induced phase transition towards wormlike micelles and gelification can then occur before the competitive micelle-to-vesicle transition, classically observed upon acidification in the absence of metal ions.[39,41] The content of COO^{-} may then still be important even at a formally acidic pH. This scenario could be the case for gels containing Al^{3+} or Fe^{2+}. *In situ* SAXS experiments[54] show that the sphere-to-wormlike transition occurs when the pH is still above 6 and that worms are stable below this pH, where vesicles are otherwise formed in the absence of metal ions.[39,41] However, if the acido-base reaction of G-C18:1 is fast, there will not be enough carboxylates to interact with the metal species at acidic pH, and gelification does not occur. In this case, pH must be increased, as found for Co^{2+} or Cr^{2+}. It is not excluded that this process is influenced by the rate of addition of the metal ion solution, in analogy to the impact of the rate of pH variation during the gelification process of sophorolipids.[27] Further work is certainly needed to better understand and control the gelification of G-C18:1.

In spite of a full understanding of the mechanisms, the metallogel properties of G-C18:1 microbial glucolipid can be exploited to test their water purification from heavy metals,[86] thus opening the perspective of this biobased molecule to water remediation, by acting as a flocculent for heavy metals, similarly as other biosurfactants[31,34] and thus possibly replacing petrochemical surfactants.[71,72]

Conclusions

In this work we explore the accessible self-assembly properties of a bolaform glucolipid microbial amphiphile composed by free-standing COOH group, an unsaturated C18:1 alkyl chain and a glucose headgroup. At the frontier between pH 6 and 7, this compound forms micelles above pH 7 and vesicles below pH 6. To its micellar phase at basic

pH, the addition of alkaline earth and transition metal ions induces a micelle-to-fiber phase transition, while addition of sodium, even in large amounts, does not induce any effect besides screening the negative charges of the micelles. Addition of salt to the vesicle phase below pH 6 induce precipitation.

A combination of SAXS and cryo-TEM shows that the gels are composed of a self-assembled fiber network (SAFIN), never reported for the specific G-C18:1 glucolipid. Cr^{2+}, Mn^{2+}, Ca^{2+} and Ag^{+} based hydrogels are composed of entangled well-defined fibers and locally forming lamellar rafts in the gel bulk. Meanwhile, Al^{3+}, Cu^{2+}, Co^{2+} and Fe^{2+} based hydrogels seem rather composed of fractal aggregates of wormlike micelles. Gelation kinetics varies across the cations, and it can be instantaneous for Ca^{2+} or it can occurs over up to 24 hours for Mn^{2+}. Other cations, like Fe^{3+}, Ni^{2+} or Zn^{2+} induce aggregation of G-C18:1 with similar structures, but they do not induce gel formation. Finally, the reactivity of other cations like Mg^{2+}, Au^{3+}, Sr^{2+}, Ba^{2+} is so high that aggregation and precipitation is observed when the cation and glucolipid solutions are put in contact. Gelation is generally observed at concentrations of the glucolipid above about 1 wt% and according to the nature of the ion, gels can reach elastic moduli higher than the kPa (e.g., Ag^{+}), comparable to many more common hydrogelators described in the literature, such as peptide derivatives.

For the most of the cations tested, the prominent role of the electrostatic interactions in the self-assembly process and gel formation is strongly suggested by the maximum gel strength reached at a ion-to-glucolipid charge ratio of 1. However, the similarity in terms of gel structure across cations with comparable speciation in solution, in addition to complementary isothermal titration calorimetry data presented in a sister work, suggest the formation of coordination complexes between the carboxylic acid of the glucolipid and the metal center, generally in the form of a free ion in solution at the pH of the experiment. This is supposed for the fibrillar metallogels with a lamellar packing of the fibers. A broader screening of the intramicellar electrostatic interactions with consequent sphere-to-wormlike transition is rather supposed for the fractal metallogels, generally observed for those cations known to have a more complex speciation (mixture of free ions, aqueous and hydroxo species) in solution.

Due to the water thickening aspect combining to a good stimuli responsiveness and the specific effect of the cation used, the microbial glucolipid biosurfactant G-C18:1 is a potential candidate for a number of applications. In a sister work, we have tested the ability of this compound to trap heavy metals in water in a gel make it also a potential candidate for water remediation.

Acknowledgements

We thank Dr. S. Roelants at Gent University and Bio Base Europe Pilot Plant, Gent, Belgium for dealing with and shipping the G-C18:1 glycolipid. Authors kindly acknowledge the French ANR, Project N° SELFAMPHI - 19-CE43-0012-01. ESRF synchrotron is acknowledged for financial support during the beamtime associated to the proposal numbers N°MX 2311 and SC-5125. Laurent Michot (Sorbonne Université, Paris, France) is kindly acknowledged for sharing the beamtime (Proposal N°: BAG 20201118) on the SWING beamline at Soleil synchrotron, Saint-Aubin, France.

References

1. Ji, S., Xu, L., Fu, X., Sun, J. & Li, Z. Light- and Metal Ion-Induced Self-Assembly and Reassembly Based on Block Copolymers Containing a Photoresponsive Polypeptide Segment. *Macromolecules* **52**, 4686–4693 (2019).
2. Terech, P. & Weiss, R. G. Low molecular mass gelators of organic liquids and the properties of their gels. *Chem. Rev.* **97**, 3133–3159 (1997).
3. Hirst, A. R., Escuder, B., Miravet, J. F. & Smith, D. K. High-tech applications of self-assembling supramolecular nanostructured gel-phase materials: From regenerative medicine to electronic devices. *Angewandte Chemie - International Edition* **47**, 8002–8018 (2008).
4. Draper, E. R. & Adams, D. J. Low-Molecular-Weight Gels: The State of the Art. *Chem* **3**, 390–410 (2017).
5. Datta, S., Saha, M. L. & Stang, P. J. Hierarchical Assemblies of Supramolecular Coordination Complexes. *Acc. Chem. Res.* **51**, 2047–2063 (2018).
6. Brassinne, J., Bourgeois, J. P., Fustin, C. A. & Gohy, J. F. Thermo-responsive properties of metallo-supramolecular block copolymer micellar hydrogels. *Soft Matter* **10**, 3086–3092 (2014).
7. Tam, A. Y. Y. & Yam, V. W. W. Recent advances in metallogels. *Chem. Soc. Rev.* **42**, 1540–1567 (2013).
8. Westcott, A., Sumby, C. J., Walshaw, R. D. & Hardie, M. J. Metallo-gels and organo-gels with tripodal cyclotriveratrylene-type and 1,3,5-substituted benzene-type ligands. *New J. Chem.* **33**, 902–912 (2009).
9. Wei, T. *et al.* Novel smart supramolecular metallo-hydrogel that could selectively recognize and effectively remove Pb2+ in aqueous solution. *Sci. China Chem.* **55**, 2554–2561 (2012).
10. Shao, T., Falcone, N. & Kraatz, H. B. Supramolecular Peptide Gels: Influencing Properties by Metal Ion Coordination and Their Wide-Ranging Applications. *ACS Omega* **5**, 1312–1317 (2020).

11. Chen, L., McDonald, T. O. & Adams, D. J. Salt-induced hydrogels from functionalised-dipeptides. *RSC Adv.* **3**, 8714–8720 (2013).
12. Zhou, X. R., Ge, R. & Luo, S. Z. Self-assembly of pH and calcium dual-responsive peptide-amphiphilic hydrogel. *J. Pept. Sci.* **19**, 737–744 (2013).
13. Li, H., Yang, P., Pageni, P. & Tang, C. Recent Advances in Metal-Containing Polymer Hydrogels. *Macromol. Rapid Commun.* **38**, 1–9 (2017).
14. Maire du Poset, A., Zitolo, A., Cousin, F., Assifaoui, A. & Lerbret, A. Evidence for an egg-box-like structure in iron(II)-polygalacturonate hydrogels: a combined EXAFS and molecular dynamics simulation study. *Phys. Chem. Chem. Phys.* **2019-Novem**, (2019).
15. Maire Du Poset, A. *et al.* Tuning the Structure of Galacturonate Hydrogels: External Gelation by Ca, Zn, or Fe Cationic Cross-Linkers. *Biomacromolecules* **20**, 2864–2872 (2019).
16. Huynh, U. T. D., Lerbret, A., Neiers, F., Chambin, O. & Assifaoui, A. Binding of Divalent Cations to Polygalacturonate: A Mechanism Driven by the Hydration Water. *J. Phys. Chem. B* **120**, 1021–1032 (2016).
17. Assifaoui, A. *et al.* Structural behaviour differences in low methoxy pectin solutions in the presence of divalent cations (Ca2+and Zn2+): A process driven by the binding mechanism of the cation with the galacturonate unit. *Soft Matter* **11**, 551–560 (2015).
18. Vasilescu, M., Angelescu, D., Caldararu, H., Almgren, M. & Khan, A. Fluorescence study on the size and shape of sodium dodecyl sulphate-aluminium salt micelles. *Colloids Surfaces A Physicochem. Eng. Asp.* **235**, 57–64 (2004).
19. Qiao, Y., Lin, Y., Wang, Y., Li, Z. & Huang, J. Metal-driven viscoelastic wormlike micelle in anionic/zwitterionic surfactant systems and template-directed synthesis of dendritic silver nanostructures. *Langmuir* **27**, 1718–1723 (2011).
20. Lang, S. Biological amphiphiles (microbial biosurfactants). *Curr. Opin. Colloid Interface Sci.* **7**, 12–20 (2002).
21. Desai, J. D. & Banat, I. M. Microbial production of surfactants and their commercial potential. *Microbiol. Mol. Biol. Rev.* **61**, 47–64 (1997).
22. Celligoi, M. A. P. C., Silveira, V. A. I., Hipólito, A., Caretta, T. O. & Baldo, C. Sophorolipids: A review on production and perspectives of application in agriculture. *Spanish J. Agric. Res.* **18**, 1–10 (2020).
23. Moldes, A. B. *et al.* Synthetic and bio-derived surfactants versus microbial biosurfactants in the cosmetic industry: An overview. *Int. J. Mol. Sci.* **22**, 2371 (2021).
24. Ribeiro, B. G., Guerra, J. M. C. & Sarubbo, L. A. Biosurfactants: Production and application prospects in the food industry. *Biotechnol. Prog.* **36**, 1–16 (2020).
25. Baccile, N. *et al.* Self-assembly, interfacial properties, interactions with macromolecules and molecular modelling and simulation of microbial bio-based amphiphiles (biosurfactants). A tutorial review. *Green Chem.* **23**, 3842–3944 (2021).

26. Baccile, N. *et al.* Bio-based glyco-bolaamphiphile forms a temperature-responsive hydrogel with tunable elastic properties. *Soft Matter* **14**, 7859–7872 (2018).
27. Ben Messaoud, G. *et al.* pH-controlled self-assembled fibrillar network (SAFiN) hydrogels: evidence of a kinetic control of the mechanical properties. *Chem. Mater.* **31**, 4817–4830 (2019).
28. Baccile, N. *et al.* Palmitic Acid Sophorolipid Biosurfactant: From Self-Assembled Fibrillar Network (SAFiN) To Hydrogels with Fast Recovery. *Philos. Trans. A* **379**, 20200343 (2021).
29. Imura, T. *et al.* Aqueous Gel Formation from Sodium Salts of Cellobiose Lipids. *J. Oleo Sci.* **63**, 1005–1010 (2014).
30. Baccile, N., Pedersen, J. S., Pehau-Arnaudet, G. & Van Bogaert, I. N. a. Surface charge of acidic sophorolipid micelles: effect of base and time. *Soft Matter* **9**, 4911–4922 (2013).
31. Hari, O. & Upadhyay, S. K. Rhamnolipid–Metal Ions (CrVI and PbII) Complexes: Spectrophotometric, Conductometric, and Surface Tension Measurement Studies. *J. Surfactants Deterg.* **24**, 281–288 (2021).
32. Chen, M. *et al.* Influence of calcium ions on rhamnolipid and rhamnolipid/anionic surfactant adsorption and self-assembly. *Langmuir* **29**, 3912–3923 (2013).
33. Shen, H.-H. H., Lin, T.-W. W., Thomas, R. K., Taylor, D. J. F. F. & Penfold, J. Surfactin structures at interfaces and in solution: The effect of pH and cations. *J. Phys. Chem. B* **115**, 4427–4435 (2011).
34. Chen, Q. *et al.* Removal of Pb and Hg from marine intertidal sediment by using rhamnolipid biosurfactant produced by a Pseudomonas aeruginosa strain. *Environ. Technol. Innov.* **22**, 101456 (2021).
35. Mulligan, C. N. & Wang, S. Remediation of a heavy metal-contaminated soil by a rhamnolipid foam. *Eng. Geol.* **85**, 75–81 (2006).
36. Miller, R. M. Biosurfactant-facilitated remediation of metal-contaminated soils. *Environ. Health Perspect.* **103**, 59–62 (1995).
37. Herman, D. C., Artiola, J. F. & Miller, R. M. Removal of Cadmium, Lead, and Zinc from Soil by a Rhamnolipid Biosurfactant. *Environ. Sci. Technol.* **29**, 2280–2285 (1995).
38. Saerens, K. M. J., Zhang, J., Saey, L., Van Bogaert, I. N. A. & Soetaert, W. Cloning and functional characterization of the UDP-glucosyltransferase UgtB1 involved in sophorolipid production by Candida bombicola and creation of a glucolipid-producing yeast strain. *Yeast* **28**, 279–292 (2011).
39. Baccile, N. *et al.* PH-Driven Self-Assembly of Acidic Microbial Glycolipids. *Langmuir* **32**, 6343–6359 (2016).
40. Baccile, N. *et al.* Chameleonic Amphiphile: the Unique Multiple Self-Assembly Properties of a Natural Glycolipid in Excess of Water. *Submitted* https://hal.archives-ouvertes.fr/hal-03576358 (2022).

41. Baccile, N. *et al.* Self-Assembly Mechanism of pH-Responsive Glycolipids: Micelles, Fibers, Vesicles, and Bilayers. *Langmuir* **32**, 10881–10894 (2016).
42. Song, A. & Hao, J. Self-assembly of metal-ligand coordinated charged vesicles. *Curr. Opin. Colloid Interface Sci.* **14**, 94–102 (2009).
43. Glatter, O. & Kratky, O. *Small Angle X-ray Scattering*. (Academic Press, 1982).
44. Manet, S. *et al.* Structure of Bolaamphiphile Sophorolipid Micelles Characterized with SAXS, SANS, and MD Simulations. *J. Phys. Chem. B* **119**, 13113–13133 (2015).
45. Aroti, A., Leontidis, E., Dubois, M. & Zemby, T. Effects of monovalent anions of the Hofmeister series on DPPC lipid bilayers part I: Swelling and in-plane equations of state. *Biophys. J.* **93**, 1580–1590 (2007).
46. Srinivasan, V. & Blankschtein, D. Effect of Counterion Binding on Micellar Solution Behavior: 2. Prediction of Micellar Solution Properties of Ionic Surfactant-Electrolyte Systems. *Langmuir* **19**, 9946–9961 (2003).
47. Jensen, G. V., Lund, R., Gummel, J., Narayanan, T. & Pedersen, J. S. Monitoring the Transition from Spherical to Polymer-like Surfactant Micelles Using Small-Angle X-Ray Scattering. *Angew. Chemie* **126**, 11708–11712 (2014).
48. Teixeira, J. Small-angle scattering by fractal systems. *J. Appl. Crystallogr.* **21**, 781–785 (1988).
49. Tanford, C. The Hydrophobic Effect: Formation of Micelles and Biological Membranes. *Biochem. Soc. Trans.* **9**, 1–178 (1980).
50. Warriner, H. E., Idziak, S. H., Slack, N. L., Davidson, P. & Safinya, C. R. Lamellar biogels: fluid-membrane-based hydrogels containing polymer lipids. *Science (80-.).* **271**, 969–73 (1996).
51. Ben Messaoud, G. *et al.* Single-Molecule Lamellar Hydrogels from Bolaform Microbial Glucolipids. *Soft Matter* **16**, 2528–2539 (2020).
52. Cui, H., Muraoka, T., Cheetham, A. G. & Stupp, S. I. Self-Assembly of Giant Peptide Nanobelts. *Nano Lett.* **9**, 945–951 (2009).
53. Dreiss, C. A. Wormlike micelles: Where do we stand? Recent developments, linear rheology and scattering techniques. *Soft Matter* **3**, 956–970 (2007).
54. Poirier, A., Griel, P. Le, Perez, J. & Baccile, N. Cation-induced fibrillation of microbial glycolipid probed by ion-resolved in situ SAXS. *Submitted* https://hal.archives-ouvertes.fr/hal-03576366v1 (2022).
55. Poirier, A. *et al.* Self-assembled fibrillar network (SAFiN) hydrogels with β-sheet-like domains: Structure. *Submitted* https://hal.archives-ouvertes.fr/hal-03576359v1 (2022).
56. Alargova, R. G., Danov, K. D., Kralchevsky, P. A., Broze, G. & Mehreteab, A. Growth of giant rodlike micelles of ionic surfactant in the presence of Al3+ counterions. *Langmuir* **14**, 4036–4049 (1998).
57. Alargova, R. G., Ivanova, V. P., Kralchevsky, P. A., Mehreteab, A. & Broze, G. Growth of

rod-like micelles in anionic surfactant solutions in the presence of Ca2+ counterions. *Colloids Surfaces A Physicochem. Eng. Asp.* **142**, 201–218 (1998).

58. Alargova, R. G., Petkov, J. T. & Petsev, D. N. Micellization and interfacial properties of alkyloxyethylene sulfate surfactants in the presence of multivalent counterions. *J. Colloid Interface Sci.* **261**, 1–11 (2003).
59. Xu, H. *et al.* Impact of AlCl3 on the self-assembly of the anionic surfactant sodium polyethylene glycol monoalkyl ether sulfate in aqueous solution. *Langmuir* **29**, 13359–13366 (2013).
60. Poirier, A., Bizien, T., Zinn, T., Pernot, P. & Baccile, N. Self-assembled fibrillar network (SAFiN) hydrogels with β-sheet-like domains: Properties. *Submitted* https://hal.archives-ouvertes.fr/hal-03576363v1 (2022).
61. Mulligan, C. N. Sustainable Remediation of Contaminated Soil Using Biosurfactants. *Front. Bioeng. Biotechnol.* **9**, 635196 (2021).
62. Mishra, S. *et al.* Biosurfactant is a powerful tool for the bioremediation of heavy metals from contaminated soils. *J. Hazard. Mater.* **418**, 126253 (2021).
63. Baes, C. F. & Mesmer, R. E. *The Hydrolysis of Cations*. (John Wiley & Sons, Inc., 1976).
64. Bi, S., Wang, C., Cao, Q. & Zhang, C. Studies on the mechanism of hydrolysis and polymerization of aluminum salts in aqueous solution: Correlations between the 'Core-links' model and 'Cage-like' Keggin-Al13 model. *Coord. Chem. Rev.* **248**, 441–455 (2004).
65. Ringbom, A. *Complexation in Analytical Chemistry*. (John Wiley & Sons, Inc., 1963).
66. Jian-Xiao, L. V., Dong, W. & Ji-Ti, Z. Interaction mechanisms between anionic surfactant micelles and different metal ions in aqueous solutions. *J. Dispers. Sci. Technol.* **27**, 1073–1077 (2006).
67. Lincoln, S. F., Richens, D. T. & Sykes, A. G. Metal Aqua Ions. in *Comprehensive Coordination Chemistry II* 515–555 (2003).
68. Persson, I. Hydrated metal ions in aqueous solution: How regular are their structures? *Pure Appl. Chem.* **82**, 1901–1917 (2010).
69. Oda, R., Huc, I., Schmutz, M., Candau, S. J. & MacKintosh, F. C. Tuning bilayer twist using chiral counterions. *Nature* **399**, 566–569 (1999).
70. Angelescu, D., Caldararu, H. & Khan, A. Some observations on the effect of the trivalent counterion Al3+ to the self-assembly of sodium dodecyl sulphate in water. *Colloids Surfaces A Physicochem. Eng. Asp.* **245**, 49–60 (2004).
71. Paton-Morales, P. & Talens-Alesson, F. I. Effect of Competitive Adsorption of Zn 2 + on the. *Langmuir* **18**, 8295–8301 (2002).
72. Paton-Morales, P. & Talens-alesson, F. I. Na + on the Flocculation of Lauryl Sulfate Micelles. *Langmuir* **20**, 6059–6064 (2001).
73. Paton, P. & Talens-Alesson, F. I. Effect of pH on the Flocculation of SDS micelles by Al3+.

Colloid Polym. Sci. **279**, 196–199 (2001).

74. Somasundaran, P., Ananthapadmanabhar, K. P. & Celik, M. S. Precipitation-Redissolution Phenomena in Sulfonate-AlCl3 Solutions. *Langmuir* **4**, 1061–1063 (1988).
75. Kuroiwa, K., Shibata, T., Takada, A., Nemoto, N. & Kimizuka, N. Heat-Set Gel-like Networks of Lipophilic Co(II) Triazole Complexes in Organic Media and Their Thermochromic Structural Transitions. *J. Am. Chem. Soc.* **126**, 2016–2021 (2004).
76. Huang, H. Q., Wang, D. F., Zhang, T. & Huang, R. Bin. Effects of different carboxylates on Ag(I) coordination compounds with pyrazinamide and pyrazinecarbonitrile with in situ reaction ligands. *J. Mol. Struct.* **1086**, 99–108 (2015).
77. Mørch, Ä. A., Donati, I., Strand, B. L. & Skja, G. Effect of Ca 2+ , Ba 2+ , and Sr 2+ on Alginate Microbeads. *Biomacromolecules* 1471–1480 (2006). doi:10.1021/bm060010d
78. Leontidis, E. Chaotropic salts interacting with soft matter: Beyond the lyotropic series. *Curr. Opin. Colloid Interface Sci.* **23**, 100–109 (2016).
79. Piepenbrock, M. O. M., Clarke, N. & Steed, J. W. Metal ion and anion-based 'tuning' of a supramolecular metallogel. *Langmuir* **25**, 8451–8456 (2009).
80. Bairi, P., Roy, B. & Nandi, A. K. PH and anion sensitive silver(i) coordinated melamine hydrogel with dye absorbing properties: Metastability at low melamine concentration. *J. Mater. Chem.* **21**, 11747–11749 (2011).
81. Ji, W. *et al.* Metal-Ion Modulated Structural Transformation of Amyloid-Like Dipeptide Supramolecular Self-Assembly. *ACS Nano* (2019). doi:10.1021/acsnano.9b03444
82. Zhang, S., Yang, S., Lan, J., Yang, S. & You, J. Helical nonracemic tubular coordination polymer gelators from simple achiral molecules. *Chem. Commun.* 6170–6172 (2008). doi:10.1039/b813375a
83. Gobeaux, F. *et al.* Structural role of counterions adsorbed on self-assembled peptide nanotubes. *J. Am. Chem. Soc.* **134**, 723–733 (2012).
84. Kim, H. J., Zin, W. C. & Lee, M. Anion-directed self-assembly of coordination polymer into tunable secondary structure. *J. Am. Chem. Soc.* **126**, 7009–7014 (2004).
85. Qiao, Y. *et al.* Unique Temperature-Dependent Supramolecular Self-Assembly: From Hierarchical 1D Nanostructures to Super Hydrogel. *J. Phys. Chem. B* **114**, 11725–11730 (2010).
86. Poirier, A. *et al.* Biosurfactant Metallogels for Heavy Metal Water Remediation. *Submitted* https://hal.archives-ouvertes.fr/hal-03576368v1 (2022).